Dual Doping of MoP with M(Mn,Fe) and S to Achieve High Hydrogen Evolution Reaction Activity in Both Acidic and Alkaline Media

Sayed M. El-Refaei,[a, b] Patrícia A. Russo,*[a] Thorsten Schultz,[c, d] Nobert Koch,[c, d] and Nicola Pinna*[a]

Rational design of cost-effective, high performance and stable hydrogen evolution reaction (HER) electrocatalysts in both acidic and alkaline media holds the key to the future hydrogen-based economy. Herein, we introduce an effective approach of simultaneous non-metal (S) and metal (Fe or Mn) doping of MoP to achieve excellent HER performance at different pH. The catalysts show remarkable overpotentials at $-10\ mA\,cm^{-2}$ of only 65 and 68 mV in 0.5 M H_2SO_4, and 50 and 51 mV in 1.0 M KOH, respectively, as well as much higher turnover frequencies compared to undoped MoP. Furthermore, the catalysts exhibit outstanding long-term stability at a fixed current of $-10\ mA\,cm^{-2}$ for 40 h. The effects of both dopants, such as electronic structure modification and enhancement of the intrinsic activity, increase of the electrochemically active surface area, and formation of coordinatively unsaturated edge sites, act cooperatively to accelerate the HER at both pH media. Additionally, the presence of oxophilic Mn and Fe at the surface results in Mn or Fe oxide/hydroxide species that promote the dissociation of water molecules in alkaline electrolyte. This work introduces a facile and effective design principle that could pave the way towards engineering highly active HER catalysts for a wide pH range.

Introduction

Hydrogen has drawn considerable attention as a potential clean energy carrier that could replace conventional fossil fuels.[1] Electrochemical water splitting (EWS) is an appealing approach to generate hydrogen, especially if utilizing electricity produced from renewable energy sources, (e.g., sun and wind).[2] Yet, global implementation of this technology is hindered in part by the high cost of the noble metal catalysts that are currently the most efficient ones for the hydrogen evolution reaction (HER) and oxygen evolution reaction (OER) half-reactions of EWS (Pt for HER, and IrOx or RuOx for OER).[2–4] Therefore, researchers have devoted significant efforts to develop earth-abundant-based catalysts for EWS, resulting in a large library of potential catalysts.[2–5] However, in general, HER earth-abundant-based catalysts are more efficient in acidic media, while those for OER are mostly active at high pH.[2,6]

Transition-metal phosphides (TMPs) are a promising alternative to Pt, owing to their high HER activity in acid electrolytes, high conductivity and facile synthesis routes.[7–10] Molybdenum phosphide (MoP) has recently been the focus of intense investigations as a HER catalyst.[11,12] However, its activity in acidic media is still inferior to that of the Pt/C benchmark, and it is unsatisfactorily low in alkaline media.[11,12] The reason for the generally significant difference in the activities of catalysts under different pH conditions is the distinct HER mechanisms. It is well accepted that the first step during HER in acidic media is a proton electrochemical adsorption (Volmer reaction), followed by the Tafel reaction or Heyrovsky desorption step to produce a H_2 molecule. In alkaline media, free protons are no longer available, and the first step (Volmer step: $H_2O + e^- \leftrightarrow H_{ads} + OH^-$) involves the dissociation of a water molecule and desorption of OH^-, and is energetically demanding.[8,13] Moreover, the exact HER mechanism in alkaline media is still under debate, further hindering the design of catalysts.[13–15]

Several strategies have been proposed to enhance the HER performance of TMPs, including metal and non-metal doping, as well as defect and hetero-interface engineering.[13] Doping TMPs with a foreign element can alter their electronic structure and lead to optimized H adsorption/desorption free energies. For instance, the HER performances of CoP[16] and NiP_2[17] in acidic medium were considerably enhanced after doping with Mn, owing to the modulation of the adsorption energies. Nevertheless, they still showed relatively low activity in alkaline

[a] S. M. El-Refaei, Dr. P. A. Russo, Prof. N. Pinna
Institut für Chemie and IRIS Adlershof
Humboldt-Universität zu Berlin
Brook-Taylor-Str. 2, 12489 Berlin (Germany)
E-mail: patricia.russo@hu-berlin.de
nicola.pinna@hu-berlin.de
[b] S. M. El-Refaei
Chemistry Department, Faculty of Science
Cairo University
Cairo 12613 (Egypt)
[c] Dr. T. Schultz, Prof. N. Koch
Institut für Physik and IRIS Adlershof
Humboldt-Universität zu Berlin
Brook-Taylor-Str. 6, 12489 Berlin (Germany)
[d] Dr. T. Schultz, Prof. N. Koch
Helmholtz-Zentrum Berlin für Materialien und Energie
Albert-Einstein-Str. 15, 12489 Berlin (Germany)

Supporting information for this article is available on the WWW under https://doi.org/10.1002/cctc.202100856

electrolyte. Similarly, S-doping of TMPs has been proven as an appealing approach to enhance their HER activity in different pH media, where the more electronegative S, compared to P, triggered a charge redistribution, in addition to an increase of the active sites exposure.[18–20] On the other hand, defect engineering such as the creation of phosphorous vacancies, was found to endow $Ni_{12}P_5$ with Pt–C like activity in alkaline medium.[21] Fe-vacancies similarly enhanced the FeP HER performance in both acidic and alkaline media.[22] An approach to boost the HER performance in alkaline medium is combining the TMP with a metal oxide/hydroxide, the latter providing H_2O dissociation centers, as reported for CoP/CeO_2,[23] NiP_2/NiO[24] and Ni_2P/MoO_2/NF HNRs.[25] This strategy was first reported by Markovic *et al.*, who presented a hybrid catalyst consisting of Pt and $Ni(OH)_2$, the latter as promoter for the sluggish Volmer step in alkaline electrolyte.[15,26] Achieving TMPs catalysts with suitable HER performance in both acidic and alkaline media is therefore challenging, as it may require the combination of several promoting strategies in a harmonized way. For example, the combination with metal oxides promotes the alkaline HER, but an excess of metal oxide can block active sites and decrease the electrical conductivity, which hinders the electron transport at high current density. Producing efficient bifunctional TMP catalysts for acidic and alkaline HER through a single approach, such as doping, is appealing from a synthetic point of view. However, this requires dopants that can promote hydrogen formation at low pH and at the same time provide water dissociation centres in basic medium. To the best of our knowledge, this has not been successfully accomplished for TMPs.

The activity of MoP in acid electrolytes has been found to improve by doping with transition-metals or non-metals such as sulfur.[27,28] Zhang *et al.* reported the suitability of Ni and Co dopants to alter the MoP electronic structure, leading to a significant activity enhancement in acid electrolyte, although not in alkaline medium.[28] It can be hypothesized that transition-metal dopants with a more oxophilic character (e.g. Mn and Fe), i.e. a stronger tendency to form oxides than phosphides, could result in the formation of enough oxide species at the surface to promote the HER activity of the phosphide in alkaline media. Such small amount of oxide, homogenously distributed at the surface, would also minimize the blocking of phosphide active sites and limit conductivity drops. However, the oxophilic nature of the dopant can lead to higher rates of dissolution in acidic electrolytes. To counter-balance this effect, a second non-metal dopant, such as sulfur can be incorporated to partially replace phosphorus. In addition to modulating the electronic structure, S-doping can generate new active sites and increase the overall number of active sites exposed by increasing the electrochemical active surface area (ECSA) of the material. All of these effects can benefit not only the HER activity in acid medium but in alkaline ones as well.

Based on the above hypotheses, we present here a strategy to tune the HER performance of MoP at both low and high pH, by simultaneously doping with S and Mn or Fe. The dual doping leads to highly active MoP catalysts supported on nickel foam (NF), requiring only overpotentials of 66–68 and 50–51 mV to drive a current density of 10 $mA\,cm^{-2}$ in 0.5 M H_2SO_4 and 1.0 M KOH, respectively. The excellent electrochemical behavior is attributed to an increase of the intrinsic activity of the catalytic sites due to electronic effects caused by the dopants, the generation of additional active sites, increase of the ECSA, and presence of surface species that accelerate the Volmer step of the HER at high pH. The catalysts also exhibit long-term stability in acidic and alkaline media.

Results and discussion

Mn,S and Fe,S dual-doped MoP catalysts were synthesized in a single step by reductive pyrolysis of the corresponding Mn,Mo- and Fe,Mo-phosphonates, using elemental sulfur as S source, as illustrated in Figure 1. Metal phosphonates were chosen as precursors to benefit from the homogeneous distribution of the metals across the phosphonate network, which can promote a homogeneous distribution of the dopants after pyrolysis.[7,29]

The effect of each dopant on the chemical, physical and electrochemical properties of MoP was first studied separately.

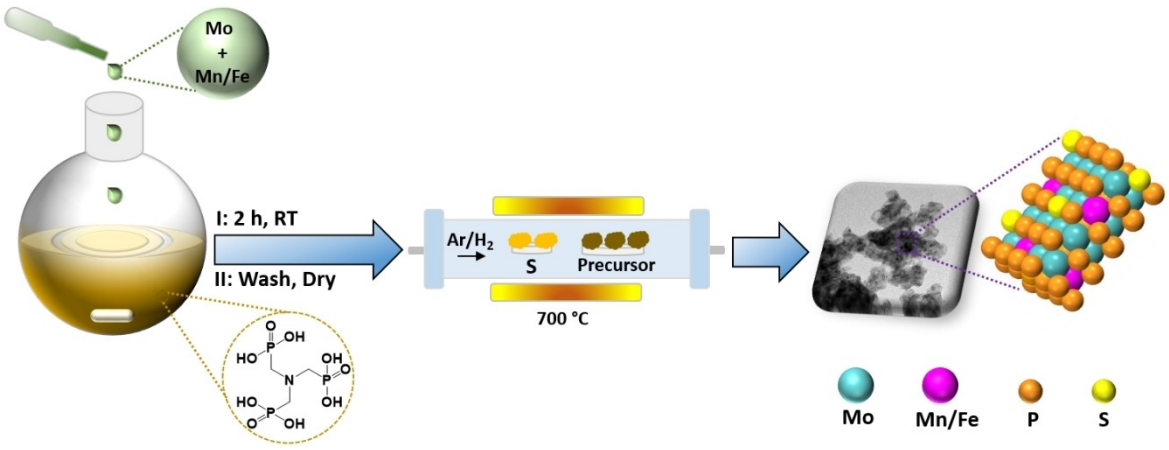

Figure 1. Schematic illustration of the synthesis of the Mn,S- (MMPS) and Fe,S-doped (FMPS) MoP electrocatalysts.

The optimum amounts of dopants were then selected to design the dual-doped catalysts, which were subsequently investigated in depth. Parallel experiments were carried out for Mn- and Fe-doping, with similar qualitative results found for both sets of samples.

MoP was doped with nominal amounts of 3, 5, and 10% Mn or Fe (denoted M3–MoP, M5–MoP, and M10–MoP, respectively, with M=Mn or Fe). The amounts of dopant incorporated were determined by energy dispersive X-ray spectroscopy (EDS), and are close to the nominal values (Table S1 and Figures S1 and 2). The X-ray powder diffraction (XRD) patterns (Figures S1, S2) show exclusively the formation of hexagonal MoP for doping levels of 3 and 5%, suggesting the successful incorporation of the metals into the MoP structure. For 10%, small reflections from $Mn_2P_2O_7$ and FeP emerge in the diffractograms, indicating the incomplete incorporation of the metals into the MoP matrix and formation of segregated phases for the highest doping level. Crystallite size for MoP, Mn5–MoP and Fe5–MoP were extracted from the XRD patterns using the Scherrer equation (Table S2). Mn5–MoP and MoP possess similiar crystallite size (ca. 12.5 nm); however, incorporation of 5% of Fe resulted in larger crystallites (ca. 15.8 nm). Transmission electron microscopy (TEM) and high-resolution TEM (HR-TEM) do not reveal any significant changes in the microstructure of the doped samples as compared to MoP (Figures S3, S4), which consist of agglomerated nanocrystals covered with a carbon shell, derived from the pyrolysis of the organic component of the phosphonate. Elemental mapping analysis confirms the uniform distribution of the dopant in the samples (Figures S3, S4).

A preliminary evaluation of the HER behavior was done to determine the effect of each dopant separately, and thus optimize the catalytic performance of the dual-doped catalysts. The preliminary tests were carried out with a three-electrode system in 0.5 M H_2SO_4, using a glass carbon (GC) electrode and a low catalyst loading of 0.25 mg cm^{-2} (Figure S5). The HER activity of MoP is comparable to that reported in the literature.[30,31] MoP requires an overpotential of 155 mV to drive a current density of 10 mA cm^{-2} (η_{10}), and a noticeable enhancement of the activity occurs after doping with Mn or Fe. Possible explanations for the activity enhancement upon doping are: (i) modulation of the electronic structure of MoP through surface electron enrichment upon Mn/Fe doping, and conductivity enhancement of the catalyst; (ii) suppression of phosphate formation at the surface through Mn/Fe doping as compared to pure MoP, rendering more potential active sites for HER; (iii) possible dissolution of MO_x (M=Mn or Fe) species at the surface, which can create defects and expose active sites. The Linear sweep voltammetry (LSV) and electrochemical impedance spectroscopy (EIS) results show that, although all amounts of dopant improve the electrocatalytic properties, the enhancement is higher for the 5% doped materials. Therefore, the samples doped with 5% Mn or Fe were selected for further studies.

MoP was additionally doped with different amounts of sulfur, by changing the weight ratio S/Mo-phosphonate during pyrolysis. Excessive use of sulfur was avoided to minimize the crystallization of MoS_2, as the formation of MoP/MoS_2 interfaces was not the target of this work. S/Mo-phosphonate ratios of 1.5, 3 and 6 were investigated (samples are denoted MoPS-1.5, MoPS-3, and MoPS-6, respectively). X-ray photoelectron spectroscopy analysis (XPS) confirms the successful S doping (Table S1). An increasing broadening of the MoP reflections with increasing S content is observed in the XRD patterns and indicative of a gradual decrease of the crystallites sizes (Figure S7), which is also confirmed by crystallite size calculations for these samples using the Scherrer equation (Table S2). Importantly, reflections belonging to MoS_2, which is likely to crystallize under these conditions, are not seen, thus excluding the formation of MoP/MoS_2 hetero-interfaces in the samples. TEM imaging (Figure S6) shows a decrease of the size of the particles inside the carbon shell upon S-doping, in line with the observed XRD broadening and crystallites size calculations. Lattice fringes corresponding to MoP are clearly seen on the HR-TEM images, confirming that the doped MoP remains highly crystalline. The incorporation of S into the MoP matrix induced higher HER activity (Figure S8), in agreement with previous reports on S-doping of metal phosphides. The improvement can be attributed to changes in the electronic structure and local disorder created by S that generate surface defects and thus potential active sites. The samples MoPS-1.5 and MoPS-3 show the highest and identical improvement of the electrocatalytic activity, providing a ~26% decrease of η_{10} with respect to MoP. Based on the preliminary evaluation of the effect of the metal and non-metal dopants on the properties of MoP, a 5% of metal dopant (Mn, Fe) and a 1.5 or 3.0 S/metal precursor weight ratio were selected for producing the dual-doped MoP materials. Additional studies indicated that 5% Mn and 1.5 S/metal precursor lead to the best catalytic activity, while for Fe it was 5% of the metal combined with a 3.0 S/metal precursor ratio. The resultant samples are denoted MMPS and FMPS, respectively. The overpotential at −10 mA cm^{-2} of the MMPS and FMPS samples with different S-doping levels is compared in Figure S9, which was used to select the catalyst materials for further studies.

Figure 2 shows the XRD and electron microscopy characterization of MMPS. For FMPS, it is shown in Figure S10. Since the results are identical for both catalysts, only MMPS is discussed here in detail. The diffractogram in Figure 2(a) corresponds to MoP, although the reflections are slightly broader than those of pure MoP, which is caused by S-doping, as discussed above (the crystallite size decreased from 12.2 nm (MoP) to 8.3 nm (MMPS)). TEM/HR-TEM imaging was done to evaluate the morphological and structural changes caused by simultaneous metal and S doping of MoP. MMPS is composed of small nanocrystals embedded in a carbon matrix. Some fused crystallites are also seen, and the high number of grain boundaries provide areas prone to active sites exposure (Figure 2 (b), (c)). HR-TEM imaging of different regions of the sample show isolated nanocrystals with distinct lattice fringes; the calculated interplanar distances of 0.32, 0.28 and 0.21 nm are indexed to the (001), (100) and (101) lattice planes of MoP, respectively (Figure 2 d, e). Selected area electron diffraction (SAED) further confirm the polycrystalline nature of MMPS and that MoP is the main catalyst component, excluding other crystalline materials and hetero-structures (Figure 2f). Further-

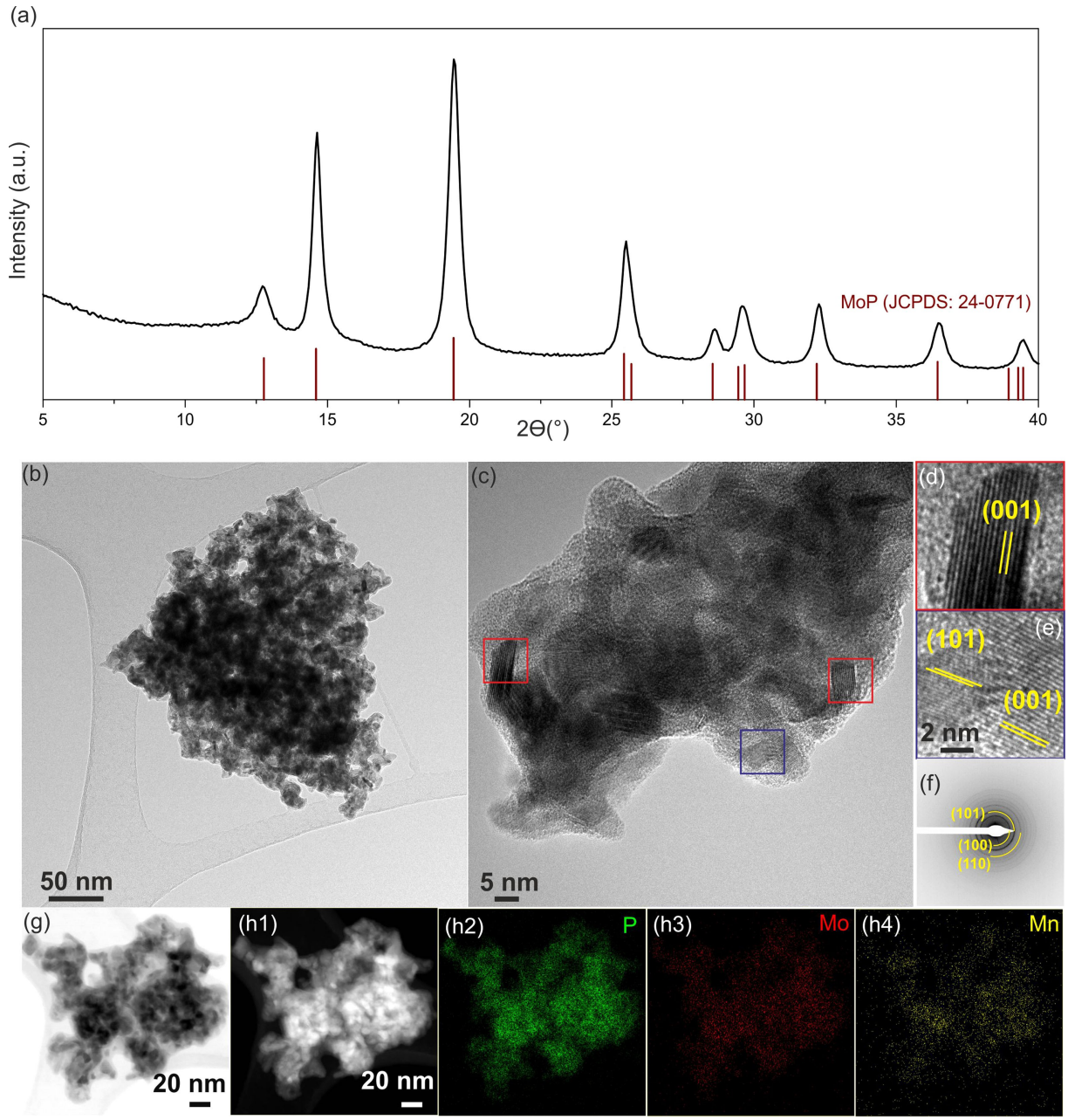

Figure 2. (a) XRD pattern, (b) TEM, (c, d and e) HR-TEM and (f) SAED pattern of MMPS. (g) HAABF, (h and h1–3) HAADF-STEM images and corresponding EDS maps of P, Mo and Mn.

more, high-angle annular dark-field scanning TEM (HAADF-STEM) coupled with EDS elemental mapping of the material (Figure2h and h1–4) reveals the homogeneous distribution of Mo, P and Mn throughout the entire selected aggregate, further indicating a successful co-doping strategy.

XPS measurements were conducted to explore the surface chemical composition and electronic states of the doped catalysts. Analyses of the MoP and single doped materials (Mn5–MoP, Fe5–MoP, MoPS-1.5, and MoPS-3) were also done as reference. The results are displayed in Figures 3 and S11–S17. The survey spectrum of MMPS (Figure S11) reveals the presence of the Mo, P, Mn and S elements at the surface, further confirming the successful dual-doping. Figures 3 a,b,c display the high-resolution Mo 3d, P 2p, and S 2p core level spectra of MMPS, which show several characteristic signals. The peaks located at 228.43 and 231.57 eV are attributed to Mo $3d_{5/2}$ and Mo $3d_{3/2}$ of $Mo^{\delta+}$ ($0 < \delta + < 4$) in the phosphide chemical state (Figure 3a).[11] The doublet at 231.73 and 234.22 eV can be assigned to Mo^{6+} in MoO_3, arising from superficial oxidation of the MoP surface.[11] Another doublet appears at 229.68 and 233.00 eV, and is attributed to Mo^{4+} in Mo–S bonds.[32] Finally, a small contribution from S 2 s at 226.27 eV is discernible in the Mo 3d spectral region.[32] The deconvolution of the S 2p spectrum gives two doublets; the one at lower binding energy

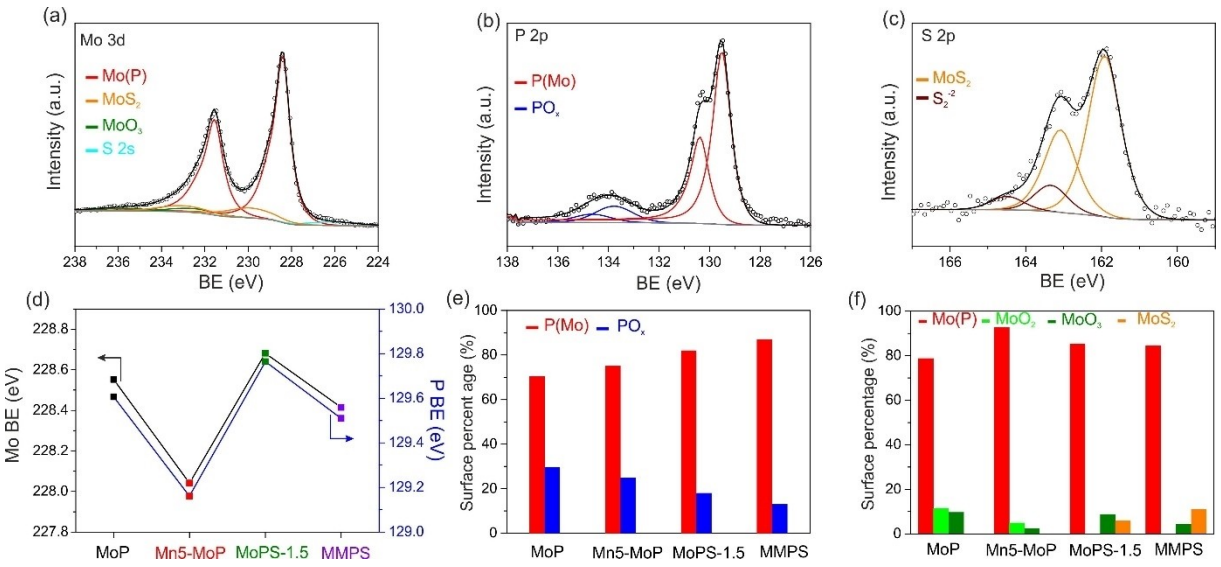

Figure 3. High resolution X-ray photoelectron spectra of (a) Mo 3d, (b) P 2p and (c) S 2p of MMPS. (d) binding energy (BE) shift of Mo 3d and P 2p; (e) phosphide and phosphates percentages and (f) Mo 3d spectra fitting components for MoP, Mn5-MoP, MoPS-1.5 and MMPS.

(161.90 and 163.00 eV) confirms the formation of Mo–S bonds, as in MoS_2 (Figure 3c).[32] The doublet at higher binding energy of 163.30 and 164.50 eV is ascribed to S_2^{2-} of unsaturated S edges in MoS_2, which are thought to be highly active sites for HER.[33] The P 2p spectrum also shows two doublets (Figure 3b). The doublet at 129.51 and 130.37 eV is ascribed to P $2p_{3/2}$ and P $2p_{1/2}$ in the phosphide chemical state, whereas the doublet at higher binding energy of 133.76 and 134.80 eV is attributed to phosphate surface species, generated from surface oxidation.[11]

To evaluate the electronic and chemical changes triggered by the doping process, the MMPS and FMPS data were compared with that of MoP and single doped materials. The deconvoluted spectra of the other samples are shown in Figures S11–16. Figure 3d summarizes the shifts in the binding energies of the Mo and P phosphide signals after doping, for the Mn,S system. Each dopant has a different effect, which can be summarized as follows: (i) doping with 5% Mn shifted both Mo(P) and P(Mo) to lower values (by about 0.51 and 0.45 eV, respectively), which suggests an electron transfer from the less electronegative Mn dopant to the MoP host; (ii) in contrast, S-doping shifts the core levels in the opposite direction, with the Mo(P) and P(Mo) peaks shifted to higher binding energy by 0.13 and 0.16 eV, respectively, implying an electron transfer from the host to the more electronegative S sites; (iii) doping simultaneously with Mn and S shifted the core levels to lower binding energy with respect to MoP, although, not as much as in the case of Mn5-MoP, which can be understood as the S electron-withdrawing effect not being enough to compensate the high electron-donating capacity of Mn. The trend is similar for the Fe,S system (Figure S17a), except that there is no significant binding energy shift for FMPS compared to MoPS-3.

The presence of Mn and/or S changes the surface chemical structure in comparison to the pristine MoP. Figure 3e compares the percentages of surface phosphide and phosphate species on MoP, Mn5–MoP, MoPS-1.5 and MMPS. The phosphide percentage increases in the order MoP < Mn5–MoP < MoP–S1.5 < MMPS. Similarly, the percentage of surface phosphate species is lower for the doped materials compared to MoP in the Fe,S system (Figure S17b). These results reflect the effect of doping in protecting the MoP surface from oxidation, which can lead to more exposed phosphide active sites for HER. Figure 3f shows the relative proportion of the fitted components of the Mo 3d spectra of MoP, Mn5-MoP, MoPS-1.5 and MMPS. The Mo(P) component accounts for 79% in the case of MoP and the rest 21% are surface oxidation species (MoO_2 and MoO_3). The presence of Mn (Mn5–MoP) supresses the surface oxidation of MoP, which is reflected in the higher Mo(P) percentage compared to MoP. Fe also has an oxidation suppression effect on MoP, although not so accentuated (Figure S17c). In the cases of the S-doped and dual doped MoP samples, the percentages of Mo(P) did not increase as much as found for the metal doped MoP materials. However, this is also due to signal overlap with that of MoS_2, which affects the estimates. Nevertheless, the S-doped and dual doped materials are still more resistant to surface oxidation than MoP, since these compounds contain lower amounts of oxidation products. The suppression of phosphate formation at the surface upon metal-doping is attributed to the oxidation of the oxophilic Mn or Fe element that acts as sacrificial agent for MoP. This is supported by the Mn 2p and Fe 2p spectra (Figures S12, S16), which show mainly oxide species at the surface instead of phosphide. Another supporting point is the binding energy shift to lower values caused by Mn- or Fe-doping, implying that the metal promotes the MoP state rather than more oxidized states. Similarly, MoPS-1.5 and MoPS-3 have lower percentage of surface phosphates compared to MoP. This phenomena has been reported before in the literature, where it the mutual stabilizing effect of P/S doping in FeS_2/FeP against

oxidation was emphasized.[34] Mn/Fe and S co-doping act jointly in suppressing the surface formation of phosphate species, which can render more active sites in MMPS and FMPS.

A comprehensive investigation of the HER performance of the dual-doped catalysts was performed in both acidic and alkaline media, together with that of pure MoP and the single doped samples, which help rationalizing the activity of the dual-doped catalysts. The electrocatalytic measurements were carried out in a three-electrode cell using 3D nickel foam (NF) electrodes as substrate. The results are shown in Figures 4 and 5 and Table 1. Platinum, which is used as benchmark, shows the typical high HER activity in both acidic and alkaline electrolytes. The bare NF substrate, on the contrary, exhibits negligible activity at low overpotentials.

MMPS and FMPS display excellent HER performance in acid electrolyte, requiring only overpotentials as low as 65, 150 and 280 mV (MMPS) and 68, 155 and 270 mV (FMPS) to drive current densities of 10, 100 and 400 mA cm^{-2}, respectively (Figures 4a, 5a). Those overpotentials are well below the ones of MoP (115, 233 and 357 mV), Mn5–MoP (88, 194 and 336 mV), Fe5-MoP (89, 187 and 326 mV), MoPS-1.5 (89, 194 and 340 mV), and MoPS-3 (92, 192 and 332 mV). Tafel plots were constructed from the corresponding LSV curves to gain insights into the HER kinetics and reaction mechanism (Figures 4b, 5b). MMPS and FMPS exhibit smaller Tafel slopes than MoP and the single doped catalysts (Table 1), indicating different reaction kinetics for the various materials. The smaller Tafel slopes for the doped catalysts compared to MoP demonstrates the effect of doping, especially of the dual-doping, on accelerating the HER reaction kinetics. Moreover, the 67–66 mV dec^{-1} slopes of MMPS and FMPS indicate that the HER follows a Volmer-Heyrovsky mechanism. Extrapolation of the Tafel plots to zero over-

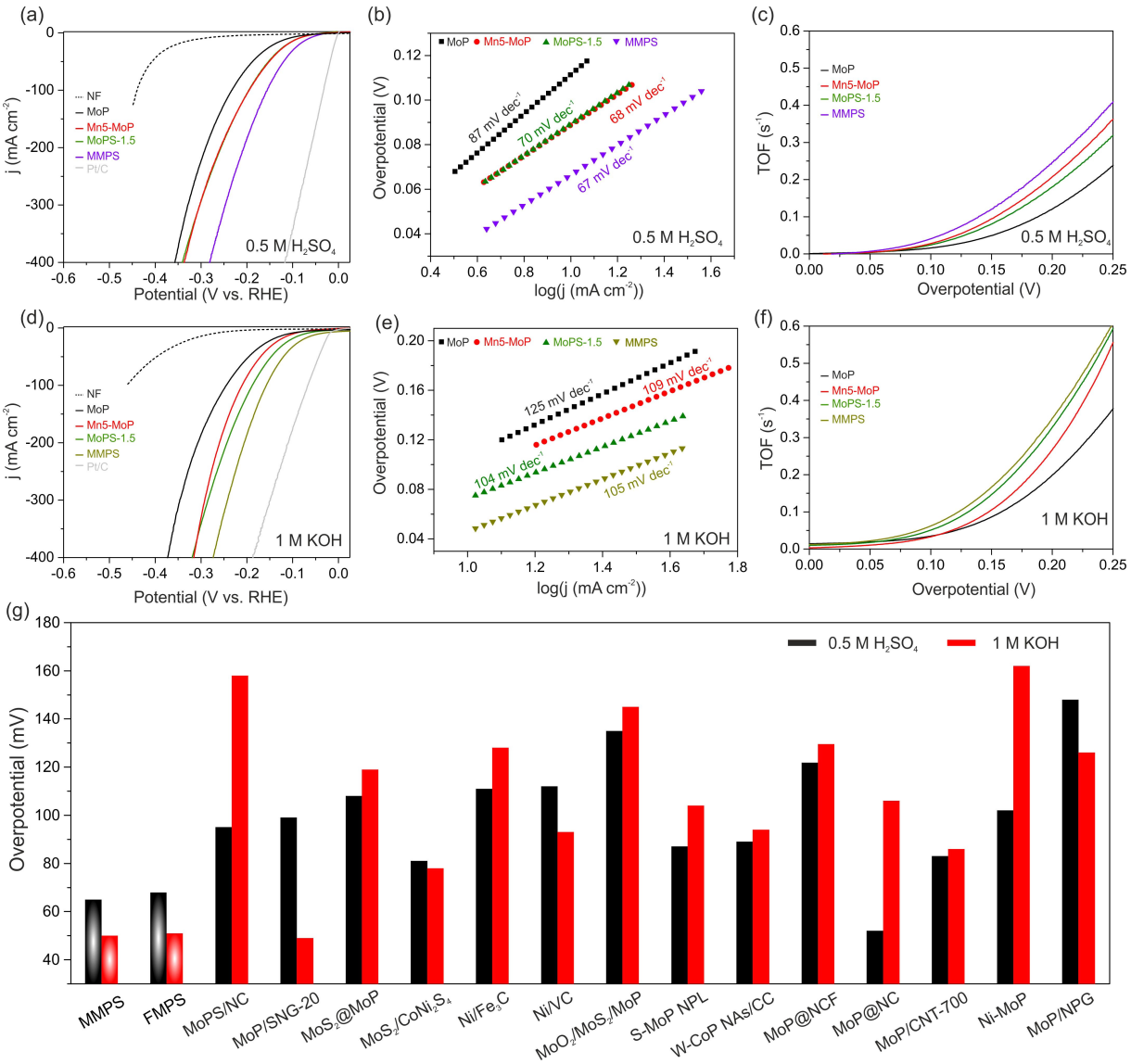

Figure 4. (a) LSV, (b) Tafel plots, and (c) TOF of MoP, single-doped and Mn,S dual doped MoP in 0.5 M H_2SO_4; (d) LSV, (e) Tafel plots, and (f) TOF of MoP, single-doped and Mn,S dual doped MoP in 1 M KOH; (g) comparison between the overpotential at 10 mA cm^{-2} of MMPS and FMPS and catalysts reported in the literature with respect to Table S3.

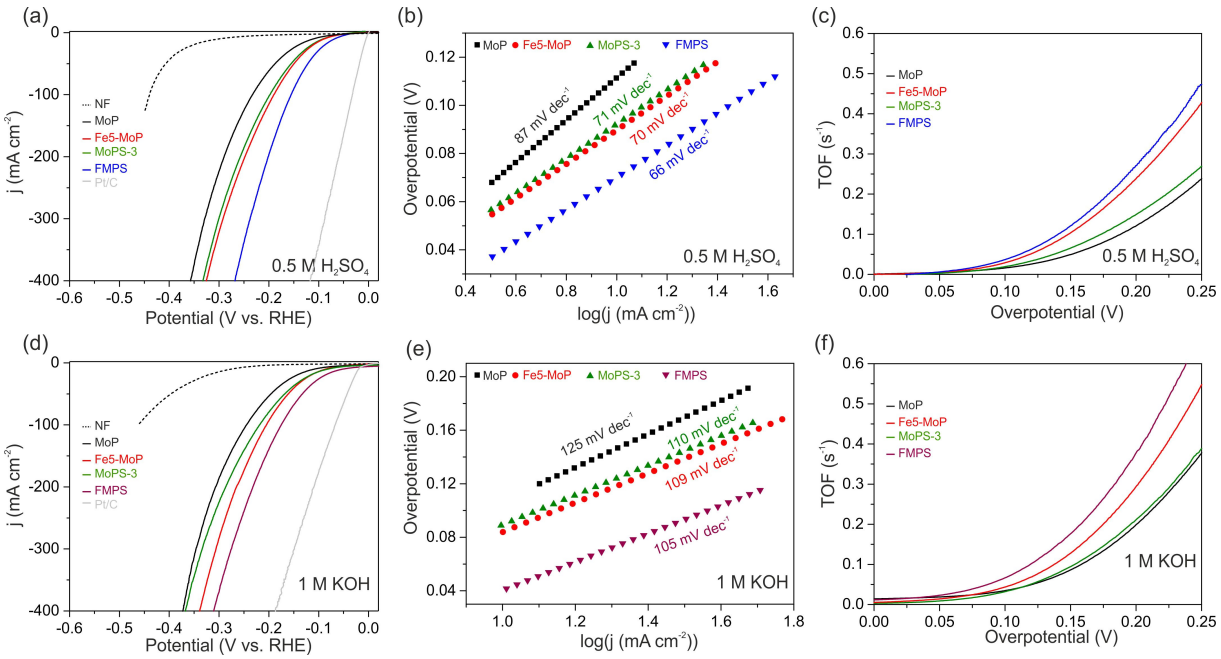

Figure 5. (a) LSV, (b) Tafel plots, and (c) TOF of MoP, single-doped and Fe,S dual doped MoP in 0.5 M H_2SO_4; (d) LSV, (e) Tafel plots, and (f) TOF of MoP, single-doped and Fe,S dual doped MoP in 1 M KOH.

Table 1. Electrochemical parameters determined for MMPS, FMPS, MoP and single doped materials in 0.5 M H_2SO_4 and 1.0 M KOH.

	0.5 M H_2SO_4					1.0 M KOH				
	η_{10} (mV)[1]	Tafel slope (mV dec^{-1})	TOF (s^{-1})[2]	C_{dl} (mF cm^{-2})[3]	j_o (mA cm^{-2})[4]	η_{10} (mV)[1]	Tafel slope (mV dec^{-1})	TOF (s^{-1})[2]	C_{dl} (mF cm^{-2})[3]	j_o (mA cm^{-2})[4]
MoP	115	87	0.12	53	0.51	111	125	0.20	27	1.39
Fe5-MoP	89	70	0.24	55	0.53	86	109	0.21	35	1.87
Mn5-MoP	88	68	0.21	58	0.55	95	109	0.27	35	1.38
MoPS-3	92	71	0.15	76	0.52	83	110	0.30	42	1.54
MoPS-1.5	89	70	0.18	65	0.55	75	104	0.33	40	1.44
FMPS	68	66	0.27	99	0.88	51	105	0.38	59	4.00
MMPS	65	67	0.25	83	1.00	50	105	0.35	58	3.50

[1] overpotential at −10 mA cm^{-2}, [2] turnover frequency at $\eta = 200$ mV; [3] double layer capacitance; [4] exchange current density.

potential gives the value of the exchange current density (j_0), which is related to the intrinsic activity of the catalysts. The j_0 value for MMPS is approximately the double of those for MoP, Mn5–MoP and MoPS-1.5 (Table 1). FMPS exhibits a smaller j_0 value than MMPS, although still significantly higher than the corresponding single doped materials. These results further demonstrate the beneficial effect of simultaneous metal and S doping on the electrocatalytic activity of MoP. EIS measurements were performed to get more information about the kinetics at the electrode/electrolyte interface. The Nyquist plots of the samples measured at the same overpotential are presented in Figure S18. The data reveals that even though the solution resistance (R_s) is generally the same for the various catalysts, the charge-transfer resistance (R_{ct}) differs, with the dual doped MoP catalysts showing R_{ct} values smaller than the other materials, indicating faster charge transfer kinetics, which correlates with the overpotential and Tafel slope trends discussed above.

The electrochemically active surface area (ECSA) is an important parameter affecting the electrochemical activity of a catalyst. The ECSA is directly proportional to the electrochemical double-layer capacitance (C_{dl}) of the electrodes, which were measured by cyclic voltammetry measurements (Figures S20–S21). As shown in Table 1, doping with Mn or Fe resulted in little changes to C_{dl} in 0.5 M H_2SO_4. On the contrary, doping with sulfur causes a more significant increase of C_{dl}, which is consistent with the decrease of the crystallites/particles sizes found through XRD and TEM analysis after S-doping. Increase of ECSA due to S-doping has been observed by other authors, and it is partially attributed to the creation of defects caused by the reaction of S with the surface of the material.[19,35] The combined effect of metal and S co-doping lead to even higher C_{dl} values for MMPS and FMPS (Table 1). This means that MMPS and FMPS have more exposed active sites at their surfaces than the other catalysts, which contributes to their superior HER performance. The ECSA-normalized LSVs (Figure S24a,c) indicate that MMPS and FMPS still exhibit higher

HER performance compared to the mono-doped and pristine MoP samples. Accordingly, the excellent HER performance of both MMPS and FMPS catalysts does not originate only from the larger ECSAs, but also from their increased intrinsic activity due to the dual doping process.

The turnover frequency (TOF) gives an estimation of the intrinsic activity of the active sites, and thus allows a rational comparison between the catalysts, excluding ECSA effects. Figures 4c and 5c display the TOF values at different overpotentials for the various catalysts in 0.5 M H_2SO_4. To calculate the TOFs, the number of active sites was determined based on the site density of a flat surface, modified with the roughness factor for each surface.[27,36,37] As Figures 4c and 5c reveal, there is a significant increase of the TOFs from the pristine MoP to the dual doped MMPS and FMPS. For example, the TOF is 0.25 s^{-1} for MMPS and 0.27 s^{-1} for FMPS at 200 mV overpotential compared to just 0.12 s^{-1} for MoP (Table 1). The results also suggest that metal doping is the most important factor contributing to the TOF increase and thus to the increase of the intrinsic activity of the catalysts in accordance with the ECSA-normalized LSVs.

The electrochemical stability of the MMPS and FMPS catalysts in acid electrolyte was evaluated through chronopotentiometry at $-10\ mA\,cm^{-2}$ and cyclic voltammetry (CV) measurements (Figure 6). The catalysts are stable under these conditions, showing a negligible overpotential decay after 40 h of continuous reaction and after 1000 CV cycles. Characterization of the spent catalysts was preformed to elucidate the possible surface changes after the stability tests. According to the HRTEM and EDS analysis, the samples were found to lose part of the metal dopant during reaction in 0.5 M H_2SO_4 due to dissolution of the Mn and Fe oxide species at the surface. (Figures S25–26; Table S1). This was expected, as the oxides of these metals are not stable against dissolution under strong acidic conditions. Nevertheless, this clearly did not negatively impact the catalytic performance, as the oxide dissolution also likely unblocked additional phosphide acid sites at the surface. Moreover, partial dissolution of Fe and Mn can lead to surface defects, as indicated by the HR-TEM. These defects are potential active sites for HER, which can compensate a possible activity deterioration from metal dopant loss during the stability test, thus making the MMPS and FMPS catalysts overall stable. XPS further disclosed the importance of the doping process in protecting the MoP surface against oxidation, as discussed above. The MoP surface was substantially oxidized after acidic HER (Figure S27), where fitting components ratios are 16, 41,

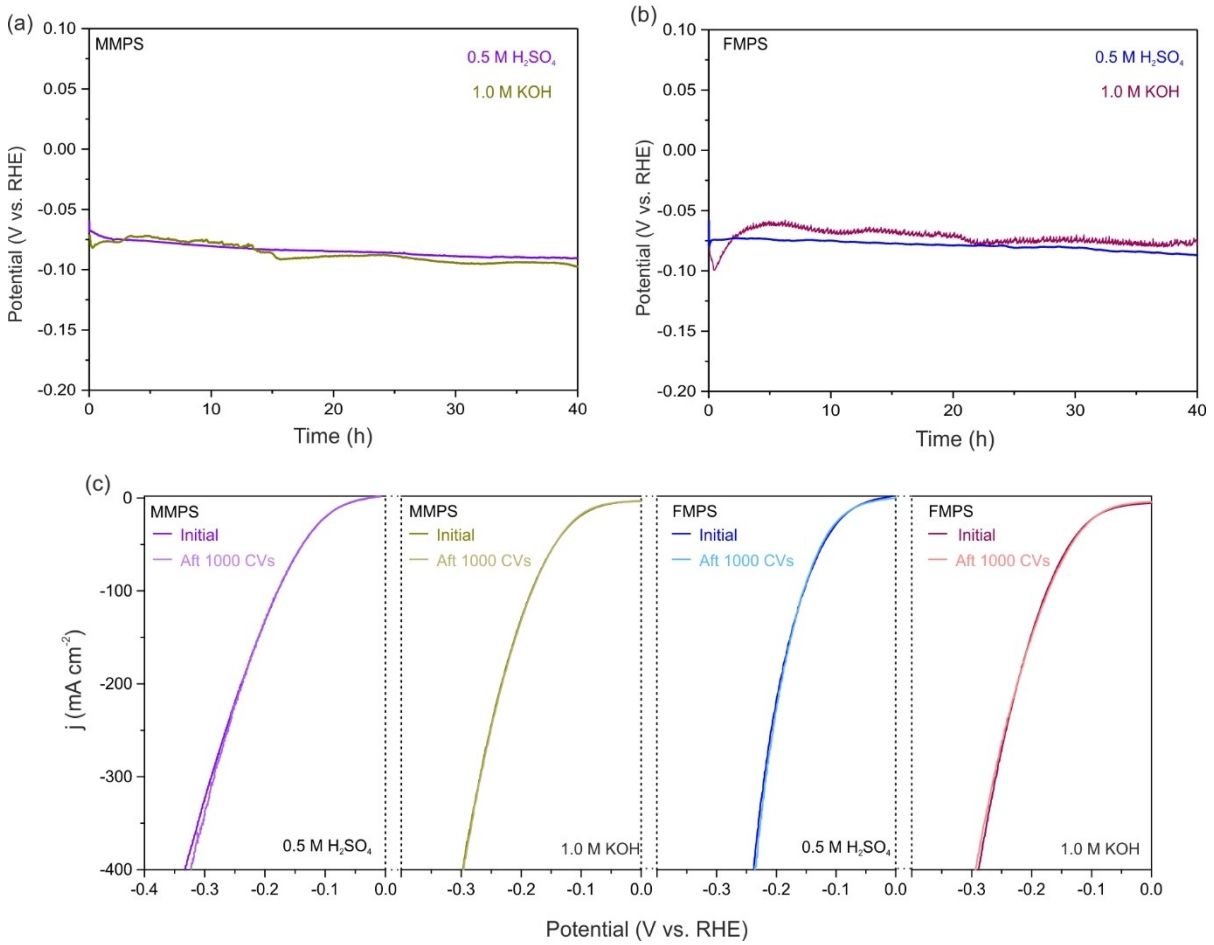

Figure 6. (a, b) i-t in 0.5 M H_2SO_4 and 1.0 M KOH for MMPS (a) and FMPS (b). (c) LSV for MMPS and FMPS in 0.5 M H_2SO_4 and 1.0 M KOH.

and 43% for MoP, MoO_2 and MoO_3 species, respectively. On the contrary, MMPS and FMPS can withstand the acidic conditions and still show a pronounced MoP proportion relative to the oxide and sulfide species. The MoP, MoS_2 and MoO_3 ratios are 64.7, 8.3 and 27% for MMPS and 74.8, 8.2, and 17% for FMPS. The oxidation resistance for the MMPS and FMPS holds true also for the phosphide to phosphate ratios, according to the P 2p spectra after reaction, where the phosphide component is still the dominant and close to the unreacted samples, in contrast to what happens with the pristine MoP (Figure S27).

The excellent performance of MMPS and FMPS at low pH results from several factors acting cooperatively. i) The metal dopants alter the electronic structure of the host MoP active sites, due to electron transfers from the dopant that leads to more electron-rich sites at the surface of the phosphide, which can promote proton adsorption and facilitate the HER in acid; transfer of electron density occurs in the opposite direction when the dopant is sulfur, although with a much smaller magnitude. This is consistent with the TOF values discussed above. Regardless of the magnitude of the effect, both types of dopants increase the charge difference between the species with partial positive charge (Mo) and partial negative charge (P) at the surface of the catalyst, which are responsible for H_2 formation at the surface. ii) Doping increases the conductivity of the catalysts and leads to faster charge-transfer at the electrode/electrolyte interface, accelerating the HER. iii) Metal and sulfur doping have a stabilizing effect on the MoP surface against oxidation. Therefore, more metal phosphide active sites are available in comparison with the undoped MoP. iv) S-doping increases the ECSA of the MoP materials due to reduction of the particles/crystallites sizes, which leads to more active sites available at the surface for reaction. S-doping additionally introduced S_2^{2-} edge sites that are considered to be highly active for HER due to their coordinatively unsaturated nature.

The samples were additionally investigated as catalysts for HER in alkaline medium (Figures 4, 5). The reaction is more challenging under these conditions, as mentioned above, due to the first step of the process involving the breaking of bonds of water molecules. Nevertheless, MMPS and FMPS display even better activity in alkaline electrolyte than in acid medium. MMPS requires overpotentials of just 50, 172 and 270 mV to reach current densities of 10, 100 and 400 mA cm^{-2}, respectively, and FMPS needs overpotentials of 51, 194 and 309 mV. These overpotentials are below those measured for MoP and the single doped MoP catalysts (Figures 4,5; Table 1). The Tafel slopes and exchange current densities estimated from the Tafel plots in Figures 4e and 5e are included in Table 1. The decrease of the Tafel slope after doping of MoP indicates the effect of the dopants in accelerating the HER kinetics also in 1.0 M KOH. The increase of the exchange current density in the same direction suggests an increase of the intrinsic activity. The charge-transfer resistances of MMPS and FMPS in alkaline medium (Figure S18) are smaller than those of the MoP and single-doped catalysts. The double-layer capacitances follow a similar trend as found for low pH (Table 1, Figures S22, S23), confirming the effect of Mn/Fe and S co-doping in increasing the exposed surface area for the HER reaction also in base. However, MMPS and FMPS still exhibit higher activity after normalizing LSVs by their ECSA, indicating that the dual doping approach enhances also their intrinsic activity (Figure S23b, d). The turnover frequency has also increased after simultaneous incorporation of S and Mn/Fe, (Table 1, Figures 4f, 5f). Additionally, MMPS and FMPS are also fairly stable after 40 h of electrolysis and 1000 CV cycles in alkaline electrolyte (Figure 6). As expected, the Mn and Fe oxide species remain on the catalysts surfaces in alkaline conditions, according to the EDX analysis of the MMPS and FMPS materials after reaction (Table S1). TEM and HR-TEM for the spent catalyst showed that MMP and FMPS still preserve their crystal and morphological structures (Figure S25–26). The corresponding EDS mapping further disclosed that the Mn and Fe dopants remained evenly distributed at the surface. Moreover, XPS analysis for MoP, MMPS and FMPS after alkaline HER showed that the dual doping strategy was important to protect MoP surface from oxidation, thus preserving the active species as discussed before in the acidic HER (Figure S27). These species can play an important role in alkaline HER, as promoters of water dissociation. The water molecules will adsorb on the oxide/hydroxide species through interaction between the oxygen with negative partial charge (–OH) and the oxide metal centers with incompletely filled 3d orbitals, while a hydrogen with positive partial charge is directed towards phosphide sites partially negatively charged, disrupting the H–OH bond of the water molecule.[24,38–40] Therefore, the catalytic efficiency of the MMPS and FMPS materials in alkaline medium is attributed to the combined effects discussed above for HER in 0.5 M H_2SO_4, together with the presence of sufficient surface oxide/hydroxide species on the catalysts to promote the dissociation of water molecules at high pH.

Achieving HER catalysts performing efficiently in both acidic and alkaline media is challenging due to differences in the mechanism and the additional functionality needed at high pH. Using a single approach like doping to achieve this purpose is even more complex. Nevertheless, the present results show that it can be accomplished by selection of suitable dopants. Figure 4g compares the overpotentials at -10 mA cm^{-2} of the MMPS and FMPS catalysts in 0.5 M H_2SO_4 and 1.0 M KOH with literature data. It shows the excellent performance of the dual-doped MoP catalysts, which compare favorably with the previous results. These also highlight the difficulty in achieving simultaneously high HER in acid and base electrolytes using the same catalyst.

Conclusion

In summary, a facile and cost-effective strategy was developed to synthesize Mn,S and Fe,S dual-doped MoP by reductive pyrolysis of the corresponding Mn,Mo- and Fe,Mo-phosphonates precursors under H_2/Ar, in the presence of elemental S. The dual doping approach resulted in a significant enhancement of the HER performance in acidic and alkaline environments. To drive -10 mA cm^{-2}, MMPS and FMPS require

65 and 68 mV in 0.5 M H_2SO_4, and 50 and 51 mV in 1.0 M KOH, respectively. These remarkable activities are fairly maintained for 40 h of continuous electrolysis at $-10\,mA\,cm^{-2}$ and after 1000 CVs in both 0.5 M H_2SO_4 and 1.0 M KOH. Thorough electrochemical characterization revealed that both MMPS and FMPS exhibit smaller Tafel slopes and charge transfer resistances than MoP, reflecting their faster HER kinetics. Moreover, MMPS and FMPS recorded higher exchange current densities and TOF values compared to MoP, which highlights the impact of dual doping in enhancing their intrinsic activity. The high activity is due to a combination of effects arising from doping, including tailoring of the electronic structure in a way that optimizes the hydrogen binding energy of both MMPS and FMPS catalysts, a prerequisite for accelerated HER. In addition, in alkaline medium, Mn and Fe surface oxide species act as water dissociation centers, providing protons for the subsequent steps. This work provides a new design strategy to develop highly active TMPs based catalysts for HER under different pH.

Experimental

Materials

All chemicals were used as received without further purifications. Nitrilotri(methylphosphonic acid) (97%), manganese chloride tetrahydrate and Nafion perfluorinated resin solution (5 wt.%) were purchased from Sigma Aldrich. Anhydrous molybdenum chloride (99.6%) and anhydrous iron chloride were purchased from ABCR. 1 N sulphuric acid and 1 N potassium hydroxide solutions for electrochemical measurements, and elemental sulfur were purchased form Carl Roth. Absolute ethanol for synthesis was purchased from vwr GMBH. Water with resistivity of $18.5\,M\Omega\,cm^{-1}$ was used in all synthesis.

Iron and manganese doped molybdenum phosphonate synthesis

In a typical synthesis, 0.245 g (0.9 mmol) of anhydrous molybdenum chloride was dissolved in 13 ml absolute ethanol under stirring. 0.150 g (0.5 mmol) of Nitrilotri(methylphosphonic acid) was dissolved in 9 ml of water, to which 9 ml absolute ethanol was added just before mixing with the molybdenum solution. After stirring for 2 hours, the precipitate was collected by centrifugation, washed with ethanol two times, and dried at 60 °C for 24 hours. To produce the Mn or Fe doped phosphonates, a suitable amount of their chloride salts (to achieve 3, 5 and 10% of doping) was dissolved in 5 ml absolute ethanol and then mixed with 8 ml of the molybdenum solution under stirring for 5 minutes. This solution was subsequently mixed with the phosphonic acid solution and stirred for 2 h.

TMPs and S-doped TMPs synthesis

Pristine and Fe/Mn doped MoP samples were prepared in one step by pyrolysis of the corresponding phosphonates, under H_2(5%)/Ar mixture at elevated temperature. Typically, 50 mg of the phosphonate precursor was placed in a ceramic boat and centred in a tubular furnace (Nabertherm), and then purged with H_2(5%)/Ar for 30 minutes before heating. Subsequently, the sample was heated with a heating ramp of $5.6\,°C\,min^{-1}$ to 700 °C, and maintained at this temperature for 3 h. After cooling to room temperature naturally, the samples were collected and grounded for further work. The samples doped with sulfur were prepared as follows: 50 mg of the metal phosphonate precursor was placed in a ceramic boat inside the tubular oven, and a certain amount of S was placed in another boat in upstream position with respect to the phosphonate. The oven was heated to 450 °C with a heating rate of $7.0\,°C\,min^{-1}$ and maintained at this temperature for 1 h, followed by heating to 700 °C with a heating rate of $4.2\,°C\,min^{-1}$ and kept at 700 °C for 3 h.

Characterizations

X-ray powder diffraction patterns were recorded using a STOE MP diffractometer in transmission mode using Mo Kα radiation ($\lambda =$ 0.07093 nm). TEM and HR-TEM micrographs were acquired on a FEI Talos F200S scanning/transmission electron microscope (S/TEM) operated at 200 kV. The X-ray photoelectron spectroscopy (XPS) measurements were performed in JEOL-JPS 9030 setup (base pressure: 3×10^{-9} mbar) using the Mg Kα radiation (1253.6 eV) generated from a twin anode X-ray source.

Electrochemical Measurements

Electrochemical measurements were performed with a Bio-Logic VMP3 potentiostat/ galvanostat having a built-in EIS analyzer. The preliminary electrochemical activity tests of the catalysts were measured in a three-electrode electrochemical cell using a 3 mm diameter glassy carbon rotating disc electrode (RDE). A graphite rod and RHE (Gaskatel), were employed as counter electrode and reference electrode, respectively. The catalyst inks were prepared as follows: 3 mg of the sample catalyst and 1 mg of carbon super P were added to 470 μL 1:1 water/ethanol and 30 μL of 5 wt % Nafion solution, and the suspension was sonicated for 30 min to obtain a homogeneous ink. The electrodes were prepared by depositing 3 μL of the catalyst ink onto the GC disc and drying at room temperature to achieve a catalyst loading of 0.25 mg cm^2. Prior to catalyst deposition, the GC electrode was polished with several grades of alumina slurry 1 μm and 0.05 μm sequentially, and then rinsed with deionized water and dried in air. The HER measurements were conducted in 0.5 M H_2SO_4 at 25 °C with the RDE rotated at 2000 rpm. Cyclic voltammetry (CV) experiments were performed in the potential window −0.3 to 0 V versus RHE with a scan rate of $20\,mV\,s^{-1}$. Linear sweep voltammetry (LSV) curves were measured in the potential window −0.4 to 0 versus RHE with a scan rate of $5\,mV\,s^{-1}$. EIS measurements were performed over a frequency range from 100 kHz to 0.1 Hz at −0.2 V versus RHE of an AC bias potential of 5 mV. Selected materials were further studied as HER catalysts in 0.5 M H_2SO_4 and 1 M KOH, using NF as catalytic support. The ink was prepared as follows:

8 mg of the catalyst and 2 mg of carbon super P were dispersed in 350 ml of 1:1 water/ethanol mixture and 50 μl of 5% Nafion solution. 60 μL of the homogenized ink were deposited on NF (0.5 cm^2 of flat area) to reach a $2.4\,mg\,cm^{-2}$ loading. The HER measurements were conducted in 0.5 M H_2SO_4 and 1 M KOH at 25 °C using the prepared sample supported NF electrode as working electrode without stirring. Cyclic voltammetry (CV) experiments were performed in the potential window −0.4 to 0 V versus RHE with a scan rate of $20\,mV\,s^{-1}$, followed by another CV in a wider potential window (−0.6 to 0 V) at $5\,mV\,s^{-1}$ to evaluate the HER performances of the series of the selected catalysts. All polarization curves were given with iR-correction. EIS measurements were conducted with the conditions mentioned earlier. The chronopotentiometric curves were measured at $-10\,mA\,cm^{-2}$ for 40 h. The accelerated CV stability test were conducted by sweeping

the potential between −0.3 and 0 V at scan rate of 200 mV s^{-1} for 1000 CVs.

Acknowledgments

S.M.E. is grateful to the Yousef Jameel Scholarship Fund. The authors thank C. Erdmann for the electron microscopy measurements. Open Access funding enabled and organized by Projekt DEAL.

Conflict of Interest

The authors declare no conflict of interest.

Keywords: doping · dual doped · hydrogen evolution reaction · molybdenum phosphide · water splitting

[1] T. R. Cook, D. K. Dogutan, S. Y. Reece, Y. Surendranath, T. S. Teets, D. G. Nocera, *Chem. Rev.* **2010**, *110*, 6474–6502.
[2] Y. Jiao, Y. Zheng, M. Jaroniec, S. Z. Qiao, *Chem. Soc. Rev.* **2015**, *44*, 2060–2086.
[3] M. S. Faber, S. Jin, *Energy Environ. Sci.* **2014**, *7*, 3519–3542.
[4] J. Greeley, T. F. Jaramillo, J. Bonde, I. Chorkendorff, J. K. Nørskov, *Nat. Mater.* **2006**, *5*, 909–913.
[5] S. Anantharaj, S. R. Ede, K. Sakthikumar, K. Karthick, S. Mishra, S. Kundu, *ACS Catal.* **2016**, *6*, 8069–8097.
[6] X. Li, X. Hao, A. Abudula, G. Guan, *J. Mater. Chem. A.* **2016**, *4*, 11973–12000.
[7] S. M. El-Refaei, P. A. Russo, P. Amsalem, N. Koch, N. Pinna, *ACS Appl. Nano Mater.* **2020**, *3*, 4147–4156.
[8] Y. Li, Z. Dong, L. Jiao, *Adv. Energy Mater.* **2020**, *10*, 1902104.
[9] H. Zhang, A. W. Maijenburg, X. Li, S. L. Schweizer, R. B. Wehrspohn, *Adv. Funct. Mater.* **2020**, *30*, 2003261.
[10] R. Zhang, P. A. Russo, M. Feist, P. Amsalem, N. Koch, N. Pinna, *ACS Appl. Mater. Interfaces.* **2017**, *9*, 14013–14022.
[11] P. Xiao, M. A. Sk, L. Thia, X. Ge, R. J. Lim, J.-Y. Wang, K. H. Lim, X. Wang *Energy Environ. Sci.* **2014**, *7*, 2624–2629.
[12] R. Ge, J. Huo, T. Liao, Y. Liu, M. Zhu, Y. Li, J. Zhang, W. Li, *Appl. Catal. B.* **2020**, *260*, 118196.
[13] X. Wang, Y. Zheng, W. Sheng, Z. J. Xu, M. Jaroniec, S.-Z. Qiao, *Mater. Today.* **2020**, *36*, 125–138.
[14] E. Liu, J. Li, L. Jiao, H. T. T. Doan, Z. Liu, Z. Zhao, Y. Huang, K. M. Abraham, S. Mukerjee, Q. Jia J Am, *Chem. Soc. Rev.* **2019**, *141*, 3232–3239.
[15] R. Subbaraman, D. Tripkovic, K.-C. Chang, D. Strmcnik, A. P. Paulikas, P. Hirunsit, M. Chan, J. Greeley, V. Stamenkovic, N. M. Markovic, *Nat. Mater.* **2012**, *11*, 550–557.
[16] T. Liu, X. Ma, D. Liu, S. Hao, G. Du, Y. Ma, A. M. Asiri, X. Sun, L. Chen, *ACS Catal.* **2017**, *7*, 98–102.
[17] X. Wang, H. Zhou, D. Zhang, M. Pi, J. Feng, S. Chen, *J. Power Sources.* **2018**, *387*, 1–8.
[18] K. Liang, S. Pakhira, Z. Yang, A. Nijamudheen, L. Ju, M. Wang, C. I. Aguirre-Velez, G. E. Sterbinsky, Y. Du, Z. Feng, J. L. Mendoza-Cortes, Y. Yang, *ACS Catal.* **2019**, *9*, 651–659.
[19] Y. Huang, X. Song, J. Deng, C. Zha, W. Huang, Y. Wu, Y. Li, *Appl. Catal. B.* **2019**, *245*, 656–661.
[20] Y. Qi, L. Zhang, L. Sun, G. Chen, Q. Luo, H. Xin, J. Peng, Y. Li, F. Ma, *Nanoscale.* **2020**, *12*, 1985–1993.
[21] J. Duan, S. Chen, C. A. Ortíz-Ledón, M. Jaroniec, S.-Z. Qiao, *Angew. Chem. Int. Ed.* **2020**, *59*, 8181–8186; *Angew. Chem.* **2020**, *132*, 8258–8263.
[22] W. L. Kwong, E. Gracia-Espino, C. C. Lee, R. Sandström, T. Wågberg, J. Messinger, *ChemSusChem.* **2017**, *10*, 4544–4551.
[23] R. Zhang, X. Ren, S. Hao, R. Ge, Z. Liu, A. M. Asiri, L. Chen, Q. Zhang, X. Sun, *J. Mater. Chem. A.* **2018**, *6*, 1985–1990.
[24] M.-Y. Wu, P.-F. Da, T. Zhang, J. Mao, H. Liu, T. Ling, *ACS Appl. Mater. Interfaces.* **2018**, *10*, 17896–17902.
[25] M. Yang, Y. Jiang, M. Qu, Y. Qin, Y. Wang, W. Shen, R. He, W. Su, M. Li, *Appl. Catal. B.* **2020**, *269*, 118803.
[26] N. Danilovic, R. Subbaraman, D. Strmcnik, K.-C. Chang, A. P. Paulikas, V. R. Stamenkovic, N. M. Markovic, *Angew. Chem. Int. Ed.* **2012**, *51*, 12495–12498; *Angew. Chem.* **2012**, *124*, 12663–12666.
[27] J. Kibsgaard, T. F. Jaramillo, *Angew. Chem. Int. Ed.* **2014**, *53*, 14433–14437; *Angew. Chem.* **2014**, *126*, 14661–14665.
[28] W. Xiao, L. Zhang, D. Bukhvalov, Z. Chen, Z. Zou, L. Shang, X. Yang, D. Yan, F. Han, T. Zhang *Nano Energy.* **2020**, *70*, 104445.
[29] R. Zhang, P. A. Russo, A. G. Buzanich, T. Jeon, N. Pinna, *Adv. Funct. Mater.* **2017**, *27*, 1703158.
[30] Y. Zhang, J. Yang, Q. Dong, H. Geng, Y. Zheng, Y. Liu, W. Wang, C. C. Li, X. Dong *ACS Appl. Mater. Interfaces.* **2018**, *10*, 26258–26263.
[31] Z. Guo, P. Liu, J. Liu, F. Du, L. Jiang, *ACS Appl. Mater. Interfaces* **2018**, *1*, 5437–5445.
[32] J. Kibsgaard, Z. Chen, B. N. Reinecke, T. F. Jaramillo, *Nat. Mater.* **2012**, *11*, 963–969.
[33] Z. Zheng, L. Yu, M. Gao, X. Chen, W. Zhou, C. Ma, L. Wu, J. Zhu, X. Meng, J. Hu, Y. Tu, S. Wu, J. Mao, Z. Tian, D. Deng, *Nat. Commun.* **2020**, *11*, 3315.
[34] Z. Wu, X. Li, W. Liu, Y. Zhong, Q. Gan, X. Li, H. Wang, *ACS Catal.* **2017**, *7*, 4026–4032.
[35] J. Chang, K. Li, Z. Wu, J. Ge, C. Liu, W. Xing, *ACS Appl. Mater. Interfaces.* **2018**, *10*, 26303–26311.
[36] J. Kibsgaard, C. Tsai, K. Chan, J. D. Benck, J. K. Nørskov, F. Abild-Pedersen, T. F. Jaramillo, *Energy Environ. Sci.* **2015**, *8*, 3022–3029.
[37] L. Yu, L. Wu, S. Song, B. McElhenny, F. Zhang, S. Chen, Z. Ren, *ACS Energy Lett.* **2020**, *5*, 2681–2689.
[38] B. You, Y. Zhang, Y. Jiao, K. Davey, S. Z. Qiao, *Angew. Chem. Int. Ed.* **2019**, *58*, 11796–11800; *Angew. Chem.* **2019**, *131*, 11922–11926.
[39] Y. Men, P. Li, J. Zhou, S. Chen, W. Luo, *Cell Rep.* **2020**, *1*, 100136.
[40] D. Zhou, Z. Wang, X. Long, Y. An, H. Lin, Z. Xing, M. Ma, S. Yang, *J. Mater. Chem. A.* **2019**, *7*, 22530–22538.

Manuscript received: June 14, 2021
Revised manuscript received: August 3, 2021
Accepted manuscript online: August 3, 2021
Version of record online: August 24, 2021